AIP | Applied Physics Letters

Size-dependent thermal instability and melting behavior of Sn nanowires

Ho Sun Shin, Jin Yu, and Jae Yong Song

Citation: Appl. Phys. Lett. **91**, 173106 (2007); doi: 10.1063/1.2801520
View online: http://dx.doi.org/10.1063/1.2801520
View Table of Contents: http://apl.aip.org/resource/1/APPLAB/v91/i17
Published by the American Institute of Physics.

Size-dependent thermal instability and melting behavior of Sn nanowires

Ho Sun Shin and Jin Yu
Center for Electronic Packaging Materials, Department of Materials Science and Engineering, Korea Advanced Institute of Science and Technology, Daejeon 305-701, South Korea

Jae Yong Song[a)]
Division of Advanced Technology, Korea Research Institute of Standards and Science, Daejeon 305-600, South Korea

(Received 14 August 2007; accepted 2 October 2007; published online 23 October 2007)

Thermal instability and melting behavior of tin nanowires were studied with a decrease of wire radius(r_{NW}=7–30 nm) via differential scanning calorimetry (DSC). Two sequential DSC measurements showed a $1/r_{NW}$ dependency of the melting temperature depression; the first melting temperature decreased from 502 to 486 K with $1/r_{NW}$ whereas the second one was more depressed between 0.8 and 5 K. The melting temperature difference between the first and second cycles increased linearly with $1/r_{NW}$. This variation was attributed to fragmentation of nanowires due to Rayleigh instability. Here, fragmentation of long nanowires was suppressed by a template confinement, resulting in the formation of short nanorods. © *2007 American Institute of Physics*. [DOI: 10.1063/1.2801520]

One-dimensional nanostructures are considered promising candidates for future nanoscale devices, which are expected to have considerably reduced size.[1,2] In relation to this, extensive studies have been performed on the effects of nanowire size on thermal stability,[3] Young's modulus,[4] tensile/yield strengths,[5] and melting/freezing temperature.[6–9] Metallic nanowires (NWs) are candidate materials for passive interconnects in future nanodevices, and understanding of the size-dependent thermal stability as well as the melting features is a key element to realizing good metallurgical bonding and reliability of NW interconnects.

Since the work of Pawlow[10] was reported, it has been shown that the melting temperature (T_{NP}) of nanoparticles depends linearly on the reciprocal of the particle size, $T_{NP}/T_b=1-\alpha/r$. Here, the subscripts NP and b denote nanoparticle and bulk, respectively, and α is a material constant related to cohesive energy, surface tension, density, shape of the material, etc.[11–15] A similar relation between melting point and radius holds for nanowires, even though T_{NW} is typically higher than T_{NP}.[8,9,16] Cylindrical nanowires are energetically unstable, as noted by several authors,[17–19] and break into nanoparticles when the wire length exceeds the circumference and perturbations of the cylindrical radius occur; this is known as the Rayleigh instability. Recently, it was reported that metallic nanowires such as Au and Cu are periodically fragmented at temperatures lower than their melting points,[20,21] a characteristic that could be applied to patterning well-ordered metallic nanostructures.[22]

In this letter, size-dependent depression of melting points and thermal instability of tin nanowires confined within a template are reported. Since metallic NWs are often structurally supported by a template, the effect of the template on the suppression of Rayleigh instability is considered.

Two nanotemplates of anodic aluminum oxide (AAO) were made out of Al foil (99.99%) by a two-step anodization process at 274 K;[23] one nanotemplate is produced in sulfuric acid (1.5M) at 15 V, and the other in oxalic acid (0.3M) at 40 V, thus creating nanotemplates (4 μm thick) with two initial pore radii (r_{NW}=7 and 15 nm). Pores were subsequently widened to have final radii of r_{NW}=10, 20, 25, and 30 nm in phosphoric acid (0.1M, 303 K). In addition, the barrier oxide layer between the pore bottom and the aluminum substrate was thinned to 5 nm by a voltage reduction process[24] for the purpose of subsequent electrodeposition.

Electrochemical deposition of Sn nanowires into the nanotemplate was accomplished using two electrodes system with a Pt counter electrode at room temperature under a sine wave voltage (V_{max}=0 V, V_{min}=−10 V, 100 Hz) in an aqueous solution (18.8 g/l $SnSO_4$ and 25 g/l H_3BO_3, pH 1.8). The NW length was controlled to 1–2.5 μm by changing the deposition time (10–30 s), and the NW diameter was estimated from three separate measurements of ten nanopores from various locations of the AAO template using scanning electron microscope (SEM).

Crystalline structure of the nanowires was analyzed using x-ray diffraction (XRD) (Cu $K\alpha$, θ-2θ scan) and transmission electron microscopy (TEM), while differential scanning calorimetry was conducted to measure T_{NW} of Sn nanowires embedded in the templates (heating rate of 3 K/min under N_2 gas). Melting points were determined from the onset temperatures of endothermic peaks in the first and second heating cycles to 510 K, and an average value out of three specimens was used. The template was removed in NaOH solution (pH 12) for the sake of preparing TEM specimens of NWs.

SEM micrographs of Sn nanowires with radii of 7 and 15 nm (denoted as 7 Sn NW and 15 Sn NW, respectively) are presented in Figs. 1(a) and 1(b). It can be seen that the 7 Sn NW has a disordered and bifurcated structure compared to the 15 Sn NW, which shows a well aligned array structure. Subsequent TEM and XRD analyses in Fig. 1(c) revealed that both NWs are single crystals with the [200] direction along the pore axis.

Melting temperatures (T_{NW}) of Sn nanowires during the first and second heating cycles were normalized against that

[a)]Author to whom correspondence should be addressed. Tel: +82-42-868-5787. FAX: +82-42-868-5032. Electronic mail: jysong@kriss.re.kr

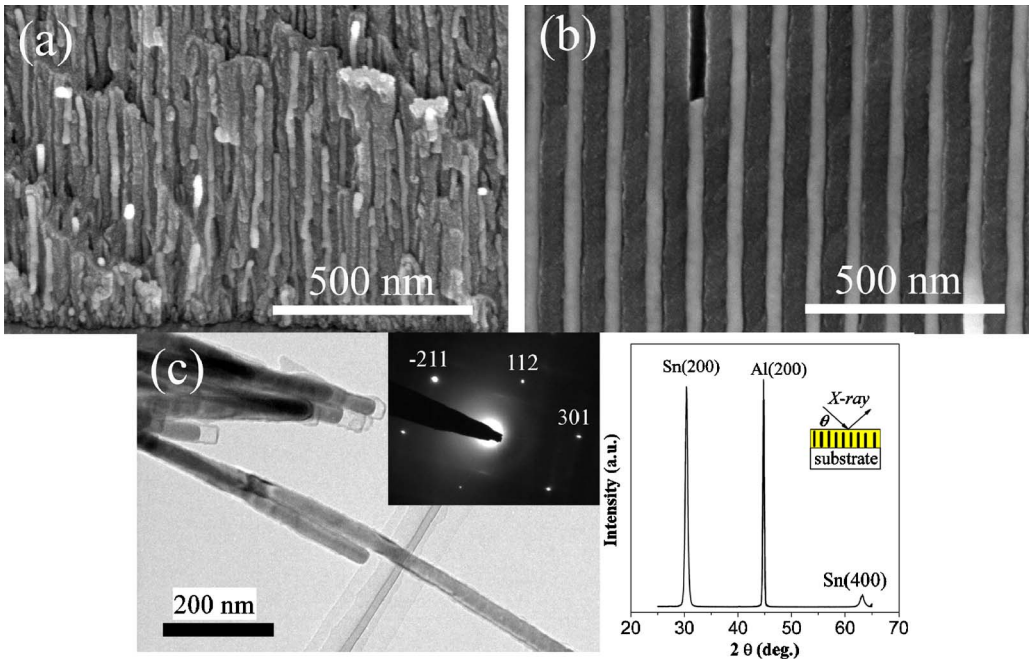

FIG. 1. Cross-sectional SEM images of as-prepared Sn nanowires with radii of (a) 7 and (b) 15 nm, and (c) typical bright field image, electron diffraction pattern of TEM, and XRD pattern of 15 Sn NW (1.5 μm). The inset in XRD pattern depicts the geometry of θ-2θ scan.

(T_b=505 K) of bulk Sn and are plotted as functions of the inverse of the wire radius ($1/r_{\mathrm{NW}}$) in Fig. 2. As the wire radius decreased from 30 to 7 nm, the first melting points ($T_{\mathrm{NW},1}$) linearly decreased from 502 to 486 K, as denoted by the solid circle data in Fig. 2. This trend is in agreement with previous results, indicating that the melting temperatures (T_{NP}) of Sn nanoparticles are depressed with decreasing radius.[11,15] The second melting temperatures ($T_{\mathrm{NW},2}$), which were measured during the subsequent second differential scanning calorimetry (DSC) cycle for the same Sn NWs, decreased with the reciprocal radius (open circle data in Fig. 2). It should be noted that the difference ($\Delta T_m = T_{\mathrm{NW},1} - T_{\mathrm{NW},2}$) between the first and second melting points showed a linear correlation with the reciprocal radius, i.e., the melting points were systematically lower during the first cycle than during the second cycle in a range of ΔT_m=0.8–5 K.

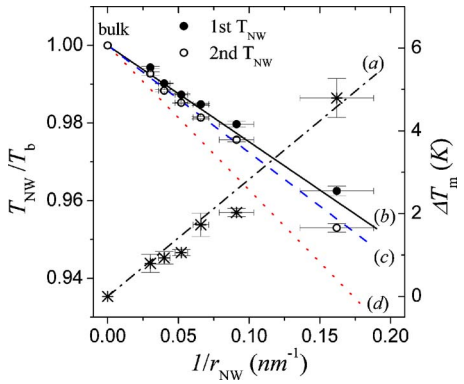

FIG. 2. The first and second melting temperatures ($T_{\mathrm{NW},1}$ and $T_{\mathrm{NW},2}$) are normalized against the bulk melting temperature and are denoted by solid and open circles, respectively. The difference (ΔT_m) between the first and second depressions is denoted by asterisks with a linear fit of the dash-dot line (a). According to Eq. (1), melting temperature depressions are theoretically predicted as a solid line (b) for long NW ($h=\infty$), a dashed line (c) for fragmented NW ($h=9r_{\mathrm{NW}}$), and a dotted line (d) for spherical nanoparticles ($h=2r_{\mathrm{NW}}$), respectively.

In Fig. 3, it can be observed that the 7 Sn and 15 Sn NWs were fragmented after the first DSC cycle up to 510 K [see Figs. 1(a) and 1(b)]. The fragmentation of Sn NWs has been ascribed to the Rayleigh instability of liquid Sn nanowire.[18,19] Also, it is noteworthy that the fragmentation of 7 Sn and 15 Sn NWs did not result in spherical nanoparticles, as predicted by the Rayleigh instability, but rather in short nanorods with a length of $h_{7\ \mathrm{Sn\ NW}}$=50–150 nm and $h_{15\ \mathrm{Sn\ NW}}$=100–600 nm, respectively. According to Nichols and Mullins, the radius of a fragmented nanoparticle is predicted to be $r_{\mathrm{NP}}=1.89r_{\mathrm{NW}}$.[19] Without a template, a freestanding nanowire would be fragmented into a chain of spherical nanoparticles, as delineated by the dashed lines in Fig. 4.[20,21] When the template confines the fragmentation of Sn NW within the pore, short nanorods with a length of $h \approx 9r_{\mathrm{NW}}$ are formed, as depicted by the solid line diagrams in Fig. 4. Here, it was assumed that the spherical nanoparticle (volume=$4\pi r_{\mathrm{NP}}^3/3$) is transformed to a nanorod (volume =$\pi r_{\mathrm{NW}}^2 h$) without a volume change. The predicted lengths (h) of fragmentation are 63 and 135 nm for the 7 Sn and 15 Sn NWs, respectively, which fall in the range of the experimentally fragmented lengths ($h_{7\ \mathrm{Sn\ NW}}$ and $h_{15\ \mathrm{Sn\ NW}}$).

As noted, $T_{\mathrm{NW},2}$ was more depressed due to the fragmentation, because the fragmented length of Sn NWs after a thermal cycle decreased with a decrease of the wire radius. In other words, ΔT_m increased linearly with the reciprocal radius; this is in agreement with a previous theoretical model describing the size and shape effects on the melting temperature of nanomaterials.[7] Under the assumptions that surface atoms are on the first layer of the nanosolid and cohesive energy is linear to the melting temperature for the material,[25] the following formula is derived:

$$\frac{T_{\mathrm{NW}}}{T_b} = 1 - \frac{N}{2n} = 1 - \frac{4r_a}{3}\left(\frac{1}{h} + \frac{1}{r_{\mathrm{NW}}}\right). \quad (1)$$

Here, N and n denote the number of surface atoms and the total atoms of a nanowire, respectively. r_a and r_{NW} denote

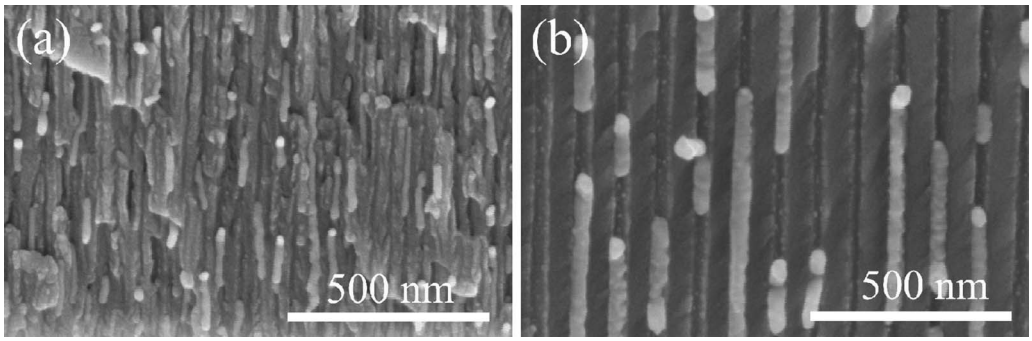

FIG. 3. Cross-sectional SEM images of (a) 7 Sn NW and (b) 15 Sn NW after the first DSC cycle up to 510 K showing that NWs are broken into short nanorods compared to the as-prepared long NWs of Fig. 1.

the atomic radius (0.186 nm for tin[14]) and the radius of the nanowire, respectively.

For as-prepared long Sn NWs, the linear depression of $T_{NW,1}$ is in accordance with the theoretical prediction (solid line, $h=\infty$), as shown in Fig. 2(b). During the first DSC cycle, as-prepared long Sn NWs were fragmented to form short nanorods depending on the wire radius, as shown in Figs. 3(a) and 3(b) and schematically described in Fig. 4. Therefore, $T_{NW,2}$ decreased more with the reciprocal radius, which is in good agreement with the theoretical prediction (denoted by dashed line, $h=9r_{NW}$) of Fig. 2(c). Both depressions are comparable with the theoretical prediction (denoted by a dotted line) of melting temperature for a spherical nanoparticle ($h=2r_{NW}$). T_{NW} was expected to approach the lowest melting point of T_{NP} with further fragmentation.

In summary, depression of the melting point of Sn NWs increased linearly with the reciprocal radius, and NWs were fragmented due to Rayleigh instability. This caused a reduction in the NW length and led to further depression of the second melting point. The NW fragmentation into spherical nanoparticles could potentially be utilized for nanopatterning; however, the fragmentation would be detrimental to the NW interconnection. The present study revealed that template supported NWs fragmented into short nanorods rather than spherical particles. This finding could provide some insight into problems related with nanowire thermal instability.

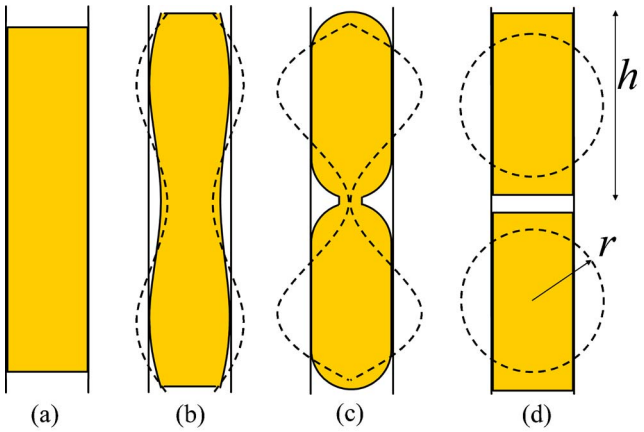

FIG. 4. A schematic diagram delineating the following: (a) A nanowire confined within a nanotemplate. (b) A perturbation in radius occurs to set in the Rayleigh intability. (c) The perturbation amplitude increases. (d) It is separated into nanorods (described by solid lines). In comparison, the dashed lines indicate that a nanowire in a template-free state breaks into particles in sequence from (a) to (d). h denotes the height of a short nanorod when a nanoparticle with a radius (r) is transformed into a nanorod without a volume change, as shown in (d).

This work was supported by the Center for Electronic Packaging Materials (ERC) of MOST/KOSEF. (Grant No. R11-2000-085-10001-0) and partly by KORP through the project of "Development of Advanced Materials Metrology."

[1] Y. Xia, P. Yang, Y. Sun, Y. Wu, B. Mayers, B. Gates, Y. Yin, F. Kim, and H. Yan, Adv. Mater. (Weinheim, Ger.) **15**, 353 (2003).
[2] F. Patolsky, B. P. Timko, G. Zheng, and C. M. Lieber, MRS Bull. **32**, 142 (2007).
[3] L. Klinger and E. Rabkin, Acta Mater. **54**, 305 (2006).
[4] C. Q. Chen, Y. Shi, Y. S. Zhang, J. Zhu, and Y. J. Yan, Phys. Rev. Lett. **96**, 0755051 (2006).
[5] F. Ma and K. W. Xu, J. Mater. Res. **21**, 2810 (2006).
[6] O. Gülseren, F. Ercolessi, and E. Tosatti, Phys. Rev. B **51**, 7377 (1995).
[7] W. H. Qi, Physica B **368**, 46 (2005).
[8] L. Miao, V. R. Bhethanabotla, and B. Joseph, Phys. Rev. B **72**, 134109 (2005).
[9] G. Abudukelimu, G. Guisbiers, and M. Wautelet, J. Mater. Res. **21**, 2829 (2006).
[10] P. Pawlow, J. Inf. Rec. Mater. **65**, 545 (1909).
[11] C. R. M. Wronski, Br. J. Appl. Phys. **18**, 1731 (1967).
[12] P. R. Couchman and W. A. Jesser, Nature (London) **269**, 481 (1977).
[13] Ph. Buffat and J.-P. Borel, Phys. Rev. A **13**, 132287 (1976).
[14] K. K. Nanda, S. N. Sahu, and S. N. Behera, Phys. Rev. A **66**, 013208 (2002).
[15] S. L. Lai, J. Y. Guo, V. Petrova, G. Ramanath, and L. H. Allen, Phys. Rev. Lett. **77**, 99 (1996).
[16] G. L. Allen, R. A. Bayles, W. W. Gile, and W. A. Jesser, Thin Solid Films **144**, 297 (1986).
[17] J. Plateau, Transl. Annual Reports of the Smithsonian Institution, 1873, p. 1863.
[18] Lord Rayleigh, Proc. London Math. Soc. **10**, 4 (1878).
[19] F. A. Nichols and Mullins, Trans. Metall. Soc. AIME **233**, 1840 (1965).
[20] M. E. Toimil Molares, A. G. Balogh, T. W. Cornelius, R. Neumann, and C. Trautmann, Appl. Phys. Lett. **85**, 5337 (2004).
[21] S. Karim, M. E. Toimil-Molares, A. G. Balogh, W. Ensinger, T. W. Cornelius, E. U. Khan, and R. Neumann, Nanotechnology **17**, 5954 (2006).
[22] J. Lian, L. Wang, X. Sun, Q. Yu, and R. C. Ewing, Nano Lett. **6**, 1047 (2006).
[23] O. Jessensky, F. Müller, and U. Gösele, Appl. Phys. Lett. **72**, 1173 (1998).
[24] R. C. Furneaux, W. R. Rigby, and A. P. Davidson, Nature (London) **337**, 147 (1989).
[25] J. H. Rose, J. Ferrante, and J. R. Smith, Phys. Rev. Lett. **47**, 675 (1981).